HPU2 Journal of Sciences:
Natural Sciences and Technology

Journal homepage: https://sj.hpu2.edu.vn

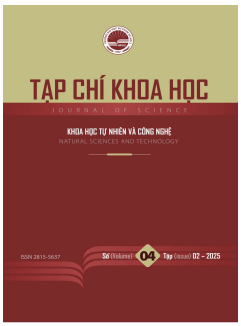

Article type: Research article

Study of the melting of FeSi interstitial alloy films by SMM

Dai-Phuong Duong[a*],Quang-Hoc Nguyen[b], Xuan-Dat Hua[b], Manh-Hung Doan[b], Minh-Hanh Pham Thi[c], Thi-Hanh Ngo[c], Thu-Hang Dao[d]

[a]*Military College of Tank Armour Officers, Phu Tho, Vietnam*
[b]*Hanoi National University of Education, Hanoi, Vietnam*
[c]*Hanoi Pedagogical University 2, Phu Tho, Vietnam*
[d]*Provincial Public Security, Phu Tho, Vietnam*

Abstract

This study utilizes the statistical moment method to investigate the effects of high temperature and pressure on the structure and melting process of Fe thin films and FeSi interstitial alloy thin films with a BCC structure. The theory is developed and validated through calculations with Fe films, then extended for application to FeSi films. When the number of layers increases to 200, corresponding to a film thickness of 70 nm, the melting temperature approaches that of the bulk material. The research results indicate that the addition of Si to FeSi films causes significant changes in melting temperature and structure, reducing the material's heat resistance.

Keywords: Fe metal thin films, FeSi interstitial alloy thin films, melting properties, temperature, high pressure, statistical moment method (SMM)

1. Introduction

Iron (Fe) is a metal characterized by low cost, high strength, and high hardness, making it widely used in many industries. However, due to its susceptibility to oxidation, Fe is often alloyed with other elements to enhance its durability. Among these, iron–silicon (FeSi) alloys are a typical example, extensively used in the production of cast iron, steel, and as a deoxidizing agent. In addition to its industrial applications, FeSi also holds potential in electronics and solid-state physics due to its unique electromagnetic properties. For example, the β-$FeSi_2$ phase is an indirect semiconductor suitable for infrared sensors, LEDs, and solar cells. With a crystal lattice compatible with silicon and the capability to

* Corresponding author, E-mail: tsphuong79@gmail.com

https://doi.org/10.56764/hpu2.jos.2025.4.2.92-104

Received date: 09-5-2025 ; Revised date: 27-6-2025 ; Accepted date: 30-7-2025

be integrated into microcircuits, FeSi is a promising candidate for spintronic devices and functional nanomaterials.

Currently, most theoretical and experimental studies on thin films mainly focus on substrate-attached materials at low temperatures and vacuum conditions [1]–[7]. Recently, the Statistical Moment Method (SMM) has been successfully applied to investigate the thermodynamic and mechanical properties of bulk materials and thin films of pure metals or alloys, such as heat capacity, thermal expansion coefficient, elastic modulus, and melting temperature [8]–[14]. However, the melting behavior of intermetallic alloys in thin film form, such as FeSi, remains a novel topic that has not yet been explored.

This study is the first to develop a statistical moment method model to investigate the melting behavior of FeSi intermetallic thin films with a BCC structure, simultaneously considering the effects of thickness, pressure, and interstitial atomic concentration. The computational results not only accurately reflect the physical trends but also provide important quantitative values to support the design of thermally stable materials under extreme conditions.

2. Theoretical basis

2.1. AB interstitial alloy model with FCC Structure

For Interstitial Alloys (IA), in principle, small, light interstitial atoms (denoted as atom B) can diffuse into any interstitial site within the crystal lattice formed by the main metal atoms (denoted as atom A), provided that the size of the interstitial site is sufficiently large. However, since the Statistical Moment Method (SMM) is favorably applied to highly symmetric systems, we propose a theoretical model below to study the deformation of AB interstitial alloys with a BCC structure, in the case where the concentration of the main metal atoms A is much greater than the concentration of interstitial atoms B. The melting problem of interstitial alloys in the form of thin films is a new and unexplored area of research.

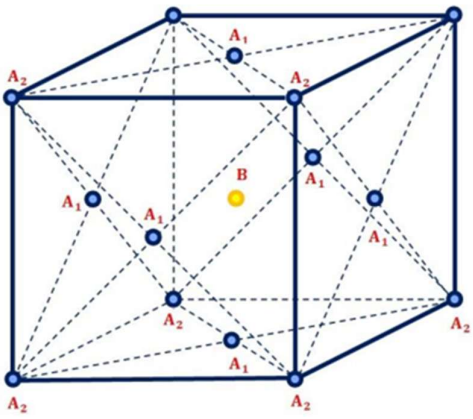

Figure 1. Ideal AB interstitial alloy model with FCC structure.

Consider Figure 1, where the interstitial atoms, denoted as B, are located at the body center, and the main metal atoms, denoted as A, are divided into two types: metal atoms A_1 positioned at the face centers, and metal atoms A_2 positioned at the corners of the unit cell.

2.2. Theory of melting of AB interstitial alloy thin films with FCC structure

2.2.1. Alloy thin film model

Consider a free-standing thin film of interstitial alloy with n^* layers and thickness d. This thin film consists of 2 atomic layers on the outer surfaces, 2 atomic layers near the outer surfaces, and n^*-4 atomic layers in the interior. Denote N_{ng}, N_{ng1} and N_{tr} as the number of atoms in the outer layer, the number of atoms in the subsurface layer, and the number of atoms in the interior layer of the thin film, respectively.

2.2.2. Binding energy, crystal parameters of the inner layer, subsurface layer, and outer layer

The binding energy u_0 and alloy parameters k, γ_1, γ_2, γ for B atoms in the two-coordination sphere approximation, and for A_1 and A_2 atoms in the three-coordination sphere approximation, belonging to the inner layer of the FCC-structured AB interstitial alloy thin film, are expressed as follows [4], [5], [15]

$$u_{0B}^{tr}=\frac{1}{2}\sum_{i=1}^{n_i}\varphi_{AB}^{tr}(r_i)=\varphi_{AB}^{tr}\left(r_{1B}^{tr}\right)+2\varphi_{AB}^{tr}\left(r_{2B}^{tr}\right),\ r_{2B}^{tr}=\sqrt{2}r_{1B}^{tr}, \tag{1}$$

$$k_B^{tr}=\frac{1}{2}\sum_i\left(\frac{\partial^2\varphi_{AB}^{tr}}{\partial u_{i\beta}^{tr2}}\right)_{eq}=\frac{1}{r_{1B}^{tr}}\frac{d\varphi_{AB}^{tr}\left(r_{1B}^{tr}\right)}{dr_{1B}^{tr}}+\frac{d^2\varphi_{AB}^{tr}\left(r_{2B}^{tr}\right)}{dr_{2B}^{tr2}}+\frac{1}{r_{2B}^{tr}}\frac{d\varphi_{AB}^{tr}\left(r_{2B}^{tr}\right)}{dr_{2B}^{tr}}, \tag{2}$$

$$\gamma_B^{tr}=4\left(\gamma_{1B}^{tr}+\gamma_{2B}^{tr}\right), \tag{3}$$

$$\gamma_{1B}^{tr}=\frac{1}{48}\sum_i\left(\frac{\partial^4\varphi_{AB}^{tr}}{\partial u_{i\beta}^{tr4}}\right)_{eq}=\frac{1}{8r_{1B}^{tr2}}\frac{d^2\varphi_{AB}^{tr}(r_{1B}^{tr})}{dr_{1B}^{tr2}}-\frac{1}{8r_{1B}^{tr3}}\frac{d\varphi_{AB}^{tr}(r_{1B}^{tr})}{dr_{1B}^{tr}}+\frac{1}{48}\frac{d^4\varphi_{AB}^{tr}(r_{2B}^{tr})}{dr_{2B}^{tr4}}+$$
$$+\frac{1}{8r_{2B}^{tr}}\frac{d^3\varphi_{AB}^{tr}(r_{2B}^{tr})}{dr_{2B}^{tr3}}-\frac{3}{16r_{2B}^{tr2}}\frac{d^2\varphi_{AB}^{tr}(r_{2B}^{tr})}{dr_{2B}^{tr2}}+\frac{3}{16r_{2B}^{tr3}}\frac{d\varphi_{AB}^{tr}(r_{2B}^{tr})}{dr_{2B}^{tr}}, \tag{4}$$

$$\gamma_{2B}^{tr}=\frac{6}{48}\sum_i\left(\frac{\partial^4\varphi_{AB}^{tr}}{\partial u_{i\alpha}^{tr2}\partial u_{i\beta}^{tr2}}\right)_{eq}=\frac{1}{4r_{1B}^{tr}}\frac{d^3\varphi_{AB}^{tr}(r_{1B}^{tr})}{dr_{1B}^{tr3}}-\frac{1}{2r_{1B}^{tr2}}\frac{d^2\varphi_{AB}^{tr}(r_{1B}^{tr})}{dr_{1B}^{tr2}}+\frac{1}{2r_{1B}^{tr3}}\frac{d\varphi_{AB}^{tr}(r_{1B}^{tr})}{dr_{1B}^{tr}}+$$
$$+\frac{1}{4r_{2B}^{tr}}\frac{d^3\varphi_{AB}^{tr}(r_{2B}^{tr})}{dr_{2B}^{tr3}}-\frac{1}{4r_{2B}^{tr2}}\frac{d^2\varphi_{AB}^{tr}(r_{2B}^{tr})}{dr_{2B}^{tr2}}+\frac{1}{4r_{2B}^{tr3}}\frac{d\varphi_{AB}^{tr}(r_{2B}^{tr})}{dr_{2B}^{tr}}, \tag{5}$$

$$u_{0A_1}^{tr}=u_{0A}^{tr}+3\varphi_{A_1B}^{tr}\left(r_{1A_1}^{tr}\right), \tag{6}$$

$$k_{A_1}^{tr}=k_A^{tr}+\frac{1}{2}\sum_i\left[\left(\frac{\partial^2\varphi_{A_1B}^{tr}}{\partial u_{i\beta}^{tr2}}\right)_{eq}\right]_{r=r_{1A_1}}=k_A^{tr}+\frac{d^2\varphi_{A_1B}^{tr}\left(r_{1A_1}^{tr}\right)}{dr_{1A_1}^{tr2}}+\frac{2}{r_{1A_1}^{tr}}\frac{d\varphi_{A_1B}^{tr}\left(r_{1A_1}^{tr}\right)}{dr_{1A_1}^{tr}}, \tag{7}$$

$$\gamma_{A_1}^{tr}=4\left(\gamma_{1A_1}^{tr}+\gamma_{2A_1}^{tr}\right), \tag{8}$$

$$\gamma_{1A_1}^{tr} = \gamma_{1A}^{tr} + \frac{1}{48}\sum_i \left[\left(\frac{\partial^4 \varphi_{A_1B}^{tr}}{\partial u_{i\beta}^{tr4}}\right)_{eq}\right]_{r=r_{1A_1}} =$$

$$= \gamma_{1A}^{tr} + \frac{1}{24}\frac{d^4\varphi_{A_1B}^{tr}\left(r_{1A_1}^{tr}\right)}{dr_{1A_1}^{tr4}} - \frac{1}{6r_{1A_1}^{tr}}\frac{d^3\varphi_{A_1B}^{tr}\left(r_{1A_1}^{tr}\right)}{dr_{1A_1}^{tr3}} + \frac{3}{4r_{1A_1}^{tr2}}\frac{d^2\varphi_{A_1B}^{tr}\left(r_{1A_1}^{tr}\right)}{dr_{1A_1}^{tr2}} - \frac{3}{4r_{1A_1}^{tr3}}\frac{d\varphi_{A_1B}^{tr}\left(r_{1A_1}^{tr}\right)}{dr_{1A_1}^{tr}}, \quad (9)$$

$$\gamma_{2A_1}^{tr} = \gamma_{2A}^{tr} + \frac{6}{48}\sum_i \left[\left(\frac{\partial^4 \varphi_{A_1B}^{tr}}{\partial u_{i\alpha}^{tr2}\partial u_{i\beta}^{tr2}}\right)_{eq}\right]_{r=r_{1A_1}} = \gamma_{2A}^{tr} + \frac{1}{4r_{1A_1}^{tr}}\frac{d^3\varphi_{A_1B}^{tr}(r_{1A_1}^{tr})}{dr_{1A_1}^{tr3}}, \quad (10)$$

$$u_{0A_2}^{tr} = u_{0A}^{tr} + 6\varphi_{A_2B}^{tr}\left(r_{1A_2}^{tr}\right), \quad (11)$$

$$k_{A_2}^{tr} = k_A^{tr} + \frac{1}{2}\sum_i \left[\left(\frac{\partial^2 \varphi_{A_2B}^{tr}}{\partial u_{i\beta}^{tr2}}\right)_{eq}\right]_{r=r_{1A_2}} = k_A^{tr} + 2\frac{d^2\varphi_{A_2B}^{tr}\left(r_{1A_2}^{tr}\right)}{dr_{1A_2}^{tr2}} + \frac{4}{r_{1A_2}^{tr}}\frac{d\varphi_{A_2B}^{tr}\left(r_{1A_2}^{tr}\right)}{dr_{1A_2}^{tr}}, \quad (12)$$

$$\gamma_{A_2}^{tr} = 4\left(\gamma_{1A_2}^{tr} + \gamma_{2A_2}^{tr}\right), \quad (13)$$

$$\gamma_{1A_2}^{tr} = \gamma_{1A}^{tr} + \frac{1}{48}\sum_i \left[\left(\frac{\partial^4 \varphi_{A_2B}^{tr}}{\partial u_{i\beta}^{tr4}}\right)_{eq}\right]_{r=r_{1A_2}} = \gamma_{1A}^{tr} + \frac{1}{24}\frac{d^4\varphi_{A_2B}^{tr}(r_{1A_2}^{tr})}{dr_{1A_2}^{tr4}} + \frac{5}{12r_{1A_2}^{tr}}\frac{d^3\varphi_{A_2B}^{tr}(r_{1A_2}^{tr})}{dr_{1A_2}^{tr3}} +$$

$$-\frac{1}{8r_{1A_2}^{tr2}}\frac{d^2\varphi_{A_2B}^{tr}(r_{1A_2}^{tr})}{dr_{1A_2}^{tr2}} + \frac{1}{8r_{1A_2}^{tr3}}\frac{d\varphi_{A_2B}^{tr}(r_{1A_2}^{tr})}{dr_{1A_2}^{tr}}, \quad (14)$$

$$\gamma_{2A_2}^{tr} = \gamma_{2A}^{tr} + \frac{6}{48}\sum_i \left[\left(\frac{\partial^4 \varphi_{A_2B}^{tr}}{\partial u_{i\alpha}^{tr2}\partial u_{i\beta}^{tr2}}\right)_{eq}\right]_{r=r_{1A_2}} = \gamma_{2A}^{tr} + \frac{1}{8}\frac{d^4\varphi_{A_2B}^{tr}(r_{1A_2}^{tr})}{dr_{1A_2}^{tr4}} +$$

$$+\frac{1}{4r_{1A_2}^{tr}}\frac{d^3\varphi_{A_2B}^{tr}(r_{1A_2}^{tr})}{dr_{1A_2}^{tr3}} + \frac{3}{8r_{1A_2}^{tr2}}\frac{d^2\varphi_{A_2B}^{tr}(r_{1A_2}^{tr})}{dr_{1A_2}^{tr2}} - \frac{3}{8r_{1A_2}^{tr3}}\frac{d\varphi_{A_2B}^{tr}(r_{1A_2}^{tr})}{dr_{1A_2}^{tr}}, \quad (15)$$

$$u_{0A}^{tr} = 4\varphi_{\mathrm{AA}}^{tr}\left(r_{1A}^{tr}\right) + 3\varphi_{\mathrm{AA}}^{tr}\left(r_{2A}^{tr}\right),\ r_{2A}^{tr} = \frac{2}{\sqrt{3}}r_{1A}^{tr}, \quad (16)$$

$$k_A^{tr} = \frac{4}{3}\frac{d^2\varphi_{\mathrm{AA}}^{tr}\left(r_{1A}^{tr}\right)}{dr_{1A}^{tr2}} + \frac{8}{3r_{1A}^{tr}}\frac{d\varphi_{\mathrm{AA}}^{tr}\left(r_{1A}^{tr}\right)}{dr_{1A}^{tr}} + \frac{d^2\varphi_{\mathrm{AA}}^{tr}\left(r_{2A}^{tr}\right)}{dr_{2A}^{tr2}} + \frac{2}{r_{2A}^{tr}}\frac{d\varphi_{\mathrm{AA}}^{tr}\left(r_{2A}^{tr}\right)}{dr_{2A}^{tr}}, \quad (17)$$

$$\gamma_{1A}^{tr} = \frac{1}{54}\frac{d^4\varphi_{\mathrm{AA}}^{tr}\left(r_{1A}^{tr}\right)}{dr_{1A}^{tr4}} + \frac{2}{9r_{1A}^{tr}}\frac{d^3\varphi_{\mathrm{AA}}^{tr}\left(r_{1A}^{tr}\right)}{dr_{1A}^{tr3}} - \frac{2}{9r_{1A}^{tr2}}\frac{d^2\varphi_{\mathrm{AA}}^{tr}\left(r_{1A}^{tr}\right)}{dr_{1A}^{tr2}} + \frac{2}{9r_{1A}^{tr3}}\frac{d\varphi_{\mathrm{AA}}^{tr}\left(r_{1A}^{tr}\right)}{dr_{1A}^{tr}} +$$

$$+\frac{1}{24}\frac{d^4\varphi_{\mathrm{AA}}^{tr}\left(r_{2A}^{tr}\right)}{dr_{2A}^{tr4}} + \frac{1}{4r_{2A}^{tr2}}\frac{d^2\varphi_{\mathrm{AA}}^{tr}\left(r_{2A}^{tr}\right)}{dr_{2A}^{tr2}} - \frac{1}{4r_{2A}^{tr3}}\frac{d\varphi_{\mathrm{AA}}^{tr}\left(r_{2A}^{tr}\right)}{dr_{2A}^{tr}}, \quad (18)$$

$$\gamma_{2A}^{tr} = \frac{1}{9}\frac{d^4\varphi_{AA}^{tr}\left(r_{1A}^{tr}\right)}{dr_{1A}^{tr4}} + \frac{2}{3r_{1A}^{tr2}}\frac{d^2\varphi_{AA}^{tr}\left(r_{1A}^{tr}\right)}{dr_{1A}^{tr2}} - \frac{2}{3r_{1A}^{tr3}}\frac{d\varphi_{AA}^{tr}\left(r_{1A}^{tr}\right)}{dr_{1A}^{tr}} + \frac{1}{2r_{2A}^{tr}}\frac{d^3\varphi_{AA}^{tr}\left(r_{2A}^{tr}\right)}{dr_{2A}^{tr3}}. \quad (19)$$

$$\gamma_{A}^{tr} = 4\left(\gamma_{1A}^{tr} + \gamma_{2A}^{tr}\right), \quad (20)$$

Where φ^{tr} is the interaction potential between two atoms belonging to the inner layer, $r_{1X}^{tr} = r_{01X}^{tr} + y_X^{tr}(T)$ and r_{01X}^{tr} are the nearest neighbor distance between atom X and another atom in the inner layer at temperatures T and 0K; $y_X^{tr}(T)$ corresponds to the displacement of atom X in the inner layer at temperature T, and n_i is the number of atoms on the i-th coordination sphere, in pure metal A, the quantities u_{0A}^{tr}, k_A^{tr}, γ_{1A}^{tr}, γ_{2A}^{tr} correspond to the BCC structure in the approximation of two coordination spheres.

Similar to the calculations above, u_0, k, γ_1, γ_2, γ for the subsurface layer and outer layer of the AB interstitial alloy thin film with a BCC structure are represented [15], [16], [17].

2.2.3. Average nearest-neighbor distance between two atoms in the inner layer, subsurface layer, and surface layer

Based on the theory of the alloy thin film model, considering the free-standing interstitial alloy thin films, pressure P, and temperature T, the average nearest neighbor distance between two X atoms in all three layers can be expressed by the following equation [15], [16], [17]

$$Pv_X = -r_{1X}\left(\frac{1}{6}\frac{\partial u_{0X}}{\partial r_{1X}} + \frac{\theta Y_X}{2k_X}\frac{\partial k_X}{\partial r_{1X}}\right), Y_X \equiv x_X \coth x_X, \quad (21)$$

Where, $v_X = \frac{4r_{1X}^3}{3\sqrt{3}}$ in the BCC structure, $\theta = k_{Bo}T, k_{Bo}$ is the Boltzmann constant, k_X is the lattice parameter, u_{0X} is the binding energy of atom X, and $x_X = \frac{\hbar\omega_X}{2\theta} = \frac{\hbar}{2\theta}\sqrt{\frac{k_X}{m_X}}, m_X$ is the atomic mass of X. Considering T at a temperature of 0K, equation (21) is expressed as follows [15], [16], [17]

$$Pv_X = -r_{1X}\left(\frac{1}{6}\frac{\partial u_{0X}}{\partial r_{1X}} + \frac{\hbar\omega_{0X}}{4k_X}\frac{\partial k_X}{\partial r_{1X}}\right). \quad (22)$$

Equation (22) can be used to calculate the nearest-neighbor distance $r_{1X}(P,0)$, lattice parameters $k_X(P,0)$, $\gamma_{1X}(P,0)$, $\gamma_{2X}(P,0)$, $\gamma_X(P,0)$, and the displacement $y_X(P,T)$ of atom X.

2.2.4. Helmholtz free energy of inner, subsurface, and outer layers

Assume that the thin film has N atoms corresponding to the n^* layer, with each layer having an equal number of atoms, which is exactly N. At that point [18],

$$N = n^* N^L \quad (23)$$

We determine the number of atoms in the inner layer N^{tr}, the subsurface layer N^{ng1}, and the outer layer N^{ng} [18]. The free energy of the thin film is determined [18]

$$\Psi = \Psi^{tr} + \Psi^{ng1} + \Psi^{ng} - TS_c = N^{tr}\psi^{tr} + N^{ng1}\psi^{ng1} + N^{ng}\psi^{ng} - TS_c =$$
$$= \left(N - 4N^L\right)\psi^{tr} + 2N^L\psi^{ng1} + 2N^L\psi^{ng} - TS_c, \quad (24)$$

With the total number of atoms in the film being $N = N^{tr} + N^{ng1} + N^{ng}$, the entropy configuration of the film is S_c, for the inner layer, the nearest outer layer, and the outer layer of the thin film, the free energy per atom are $\psi^{tr}, \psi^{ng1}, \psi^{ng}$. From equation (24), the free energy of the thin film per atom is derived [18].

$$\frac{\Psi}{N} = \left(1 - \frac{4}{n^*}\right)\psi^{tr} + \frac{2}{n^*}\psi^{ng1} + \frac{2}{n^*}\psi^{ng} - \frac{TS_c}{N}. \quad (25)$$

The symbols: $\bar{a}$ is the average nearest neighbor distance between two atoms, $\bar{b}$ is the average thickness of the two corresponding layers of the film, and $\bar{a}_c$ is the average lattice constant of the film.

Applied to the thin film with a BCC structure [18], it is given that

$$\bar{b} = \frac{\bar{a}}{\sqrt{3}}, \quad \bar{a}_c = 2\bar{b} = \frac{2\bar{a}}{\sqrt{3}}. \quad (26)$$

The thickness of the film is related to the number of layers through [18]

$$d = 2b^{ng} + 2b^{ng1} + \left(n^* - 4\right)b^{tr} = \left(n^* - 1\right)\bar{b} = \left(n^* - 1\right)\frac{\bar{a}}{\sqrt{3}}. \quad (27)$$

Therefore, [18],

$$n^* = 1 + \frac{d}{\bar{b}} = 1 + \frac{d\sqrt{3}}{\bar{a}}. \quad (28)$$

We derive the expression for the free energy [16], [17], [18]

$$\frac{\Psi}{N} = \frac{d\sqrt{3} - 3\bar{a}}{d\sqrt{3} + \bar{a}}\psi^{tr} + \frac{2\bar{a}}{d\sqrt{3} + \bar{a}}\psi^{ng} + \frac{2\bar{a}}{d\sqrt{3} + \bar{a}}\psi^{ng1} - \frac{TS_c}{N} =$$
$$= \frac{d\sqrt{3} - 3\bar{a}}{d\sqrt{3} + \bar{a}}\left(\sum_X c_X^{tr}\psi_X^{tr} - TS_c^{tr}\right) + \frac{2\bar{a}}{d\sqrt{3} + \bar{a}}\left(\sum_X c_X^{ng}\psi_X^{ng} - TS_c^{ng}\right) +$$
$$\frac{2\bar{a}}{d\sqrt{3} + \bar{a}}\left(\sum_X c_X^{ng1}\psi_X^{ng1} - TS_c^{ng1}\right) - \frac{TS_c}{N}. \quad (29)$$

2.2.5. Melting theory of AB interstitial alloy thin films with bcc structure

From the free energy, the pressure has the form of

$$P = -\left(\frac{\partial\Psi}{\partial V}\right)_T = -\frac{r_1}{3V}\left(\frac{\partial\Psi}{\partial r_1}\right)_T \approx -\frac{r_1}{3V}\left[\frac{d\sqrt{3} - 3\bar{a}}{d\sqrt{3} + \bar{a}}\sum_X c_X^{tr}\left(\frac{\partial\Psi_X^{tr}}{\partial r_{1X}^{tr}}\right)_T - \frac{2\bar{a}}{d\sqrt{3} + \bar{a}}\sum_X c_X^{ng}\left(\frac{\partial\Psi_X^{ng}}{\partial r_{1x}^{ng}}\right)_T -\right.$$
$$\left. - \frac{2\bar{a}}{d\sqrt{3} + \bar{a}}\sum_X c_X^{ng1}\left(\frac{\partial\Psi_X^{ng1}}{\partial r_{1X}^{ng1}}\right)_T\right].$$

(30)

For an ideal interstitial alloy thin film with a BCC structure

$$PV = -\frac{r_1}{6}\left[\frac{d\sqrt{3}-3\bar{a}}{d\sqrt{3}+\bar{a}}\sum_X c_X^{tr}\left(\frac{\partial U_{0X}^{tr}}{\partial r_{1X}^{tr}}+\frac{\theta X_X^{tr}}{2k_X^{tr}}\frac{\partial k_X^{tr}}{\partial r_{1X}^{tr}}\right)-\frac{2\bar{a}}{d\sqrt{3}+\bar{a}}\sum_X c_X^{ng}\left(\frac{\partial U_{0X}^{ng}}{\partial r_{1X}^{ng}}+\frac{\theta X_X^{ng}}{2k_X^{ng}}\frac{\partial k_X^{ng}}{\partial r_{1X}^{ng}}\right)-\right.$$
$$\left.-\frac{2\bar{a}}{d\sqrt{3}+\bar{a}}\sum_X c_X^{ng1}\left(\frac{\partial U_{0X}^{ng1}}{\partial r_{1X}^{ng1}}+\frac{\theta X_X^{ng1}}{2k_X^{ng1}}\frac{\partial k_X^{ng1}}{\partial r_{1X}^{ng1}}\right)\right]. \tag{31}$$

Let

$$\gamma_G = -\frac{r_1}{6}\left[\frac{d\sqrt{3}-3\bar{a}}{d\sqrt{3}+\bar{a}}\sum_X \frac{c_X^{tr}X_X^{tr}}{k_X^{tr}}\frac{\partial k_X^{tr}}{\partial r_{1X}^{tr}}-\frac{2\bar{a}}{d\sqrt{3}+\bar{a}}\sum_X \frac{c_X^{ng}X_X^{ng}}{k_X^{ng}}\frac{\partial k_X^{ng}}{\partial r_{1X}^{ng}}-\right.$$
$$\left.-\frac{2\bar{a}}{d\sqrt{3}+\bar{a}}\sum_X \frac{c_X^{ng1}X_X^{ng1}}{k_X^{ng1}}\frac{\partial k_X^{ng1}}{\partial r_{1X}^{ng1}}\right]. \tag{32}$$

Here, γ_G plays the role of the Grüneisen parameter of the interstitial alloy thin film. In that case,

$$P = -\frac{r_1}{6V}\left[\frac{d\sqrt{3}-3\bar{a}}{d\sqrt{3}+\bar{a}}\sum_X c_X^{tr}\frac{\partial U_{0X}^{tr}}{\partial r_{1X}^{tr}}-\frac{2\bar{a}}{d\sqrt{3}+\bar{a}}\sum_X c_X^{ng}\frac{\partial U_{0X}^{ng}}{\partial r_{1X}^{ng}}-\right.$$
$$\left.-\frac{2\bar{a}}{d\sqrt{3}+\bar{a}}\sum_X c_X^{ng1}\frac{\partial U_{0X}^{ng1}}{\partial r_{1X}^{ng1}}\right]+\frac{3\gamma_G\theta}{V}. \tag{33}$$

The condition for the absolute stability limit of the crystalline state is in the form of

$$\left(\frac{\partial P}{\partial V}\right)_{T_s}=0 \text{ hay } \left(\frac{\partial P}{\partial r_1}\right)_{T_s}=0. \tag{34}$$

From there, we can derive the temperature for the absolute stability limit of the crystalline state

$$T_s = \frac{TS1}{MS1},$$

Set up a similar calculation for the case when P = 0, then $T_s = \frac{TS_2}{MS_2}$ (35)

Since the curve of the absolute stability limit of the interstitial alloy thin film state approaches the melting curve of the interstitial alloy thin film, the temperature T_s is usually high and can be considered $X_X^m \equiv x_X^m \coth x_X^m \approx 1 (X = A, C, A_1, A_2, m = tr, ng, ng1)$ at temperature T_s. Therefore, we deduce

$$\frac{4}{(r_1)^2 k_B}\left[\frac{d\sqrt{3}-3\bar{a}}{d\sqrt{3}+\bar{a}}\sum_X \frac{c_X^{tr}}{\left(k_X^{tr}\right)^2}\left(\frac{\partial k_X^{tr}}{\partial r_{1X}^{tr}}\right)^2-\frac{2\bar{a}}{d\sqrt{3}+\bar{a}}\sum_X \frac{c_X^{ng}}{\left(k_X^{ng}\right)^2}\left(\frac{\partial k_X^{ng}}{\partial r_{1X}^{ng}}\right)^2-\right.$$

$$\left.-\frac{2\bar{a}}{d\sqrt{3}+\bar{a}}\sum_X \frac{c_X^{ng1}}{\left(k_X^{ng1}\right)^2}\left(\frac{\partial k_X^{ng1}}{\partial r_{1X}^{ng1}}\right)^2\right]^{-1}\left\{2PV+\frac{(r_1)^2}{6}\left[\frac{d\sqrt{3}-3\bar{a}}{d\sqrt{3}+\bar{a}}\sum_X c_X^{tr}\frac{\partial^2 U_{0X}^{tr}}{\partial\left(r_{1X}^{tr}\right)^2}-\frac{2\bar{a}}{d\sqrt{3}+\bar{a}}\sum_X c_X^{ng}\frac{\partial^2 U_{0X}^{ng}}{\partial\left(r_{1X}^{ng}\right)^2}-\right.\right.$$

$$\left.-\frac{2\bar{a}}{d\sqrt{3}+\bar{a}}\sum_X c_X^{ng1}\frac{\partial^2 U_{0X}^{ng1}}{\partial\left(r_{1X}^{ng1}\right)^2}\right]-\frac{\hbar(r_1)^2}{4}\left\{\frac{d\sqrt{3}-3\bar{a}}{d\sqrt{3}+\bar{a}}\sum_X \frac{c_X^{tr}\omega_X^{tr}}{k_X^{tr}}\left[\frac{1}{2k_X^{tr}}\left(\frac{\partial k_X^{tr}}{\partial r_{1X}^{tr}}\right)^2-\frac{\partial^2 k_X^{tr}}{\partial\left(r_{1X}^{tr}\right)^2}\right]-\right.$$

$$\left.\left.-\frac{2\bar{a}}{d\sqrt{3}+\bar{a}}\sum_X \frac{c_X^{ng}\omega_X^{ng}}{k_X^{ng}}\left[\frac{1}{2k_X^{ng}}\left(\frac{\partial k_X^{ng}}{\partial r_{1X}^{tr}}\right)^2-\frac{\partial^2 k_X^{ng}}{\partial\left(r_{1X}^{ng}\right)^2}\right]-\frac{2\bar{a}}{d\sqrt{3}+\bar{a}}\sum_X \frac{c_X^{ng1}\omega_X^{ng1}}{k_X^{ng1}}\left[\frac{1}{2k_X^{ng1}}\left(\frac{\partial k_X^{ng1}}{\partial r_{1X}^{tr1}}\right)^2-\frac{\partial^2 k_X^{ng1}}{\partial\left(r_{1X}^{ng1}\right)^2}\right]\right\}\right\}+$$

$$+\frac{1}{k_B r_1}\left[\frac{d\sqrt{3}-3\bar{a}}{d\sqrt{3}+\bar{a}}\sum_X \frac{c_X^{tr}}{k_X^{tr}}\frac{\partial k_X^{tr}}{\partial r_{1X}^{tr}}-\frac{2\bar{a}}{d\sqrt{3}+\bar{a}}\sum_X \frac{c_X^{ng}}{k_X^{ng}}\frac{\partial k_X^{ng}}{\partial r_{1X}^{ng}}-\right.$$

$$\left.-\frac{2\bar{a}}{d\sqrt{3}+\bar{a}}\sum_X \frac{c_X^{ng1}}{k_X^{ng1}}\frac{\partial k_X^{ng1}}{\partial r_{1X}^{ng1}}\right]^{-1}\left\{2PV+\frac{r_1}{3}\left[\frac{d\sqrt{3}-3\bar{a}}{d\sqrt{3}+\bar{a}}\sum_X c_X^{tr}\frac{\partial U_{0X}^{tr}}{\partial r_{1X}^{tr}}-\frac{2\bar{a}}{d\sqrt{3}+\bar{a}}\sum_X c_X^{ng}\frac{\partial U_{0X}^{ng}}{\partial r_{1X}^{ng}}-\right.\right.$$

$$\left.\left.-\frac{2\bar{a}}{d\sqrt{3}+\bar{a}}\sum_X c_X^{ng1}\frac{\partial U_{0X}^{ng1}}{\partial r_{1X}^{ng1}}\right]\right\}=0. \tag{36}$$

The equation of the absolute stability limit curve is given in (36). The pressure is considered as a function of the average nearest neighbor distance

$$P=P(r_1). \tag{37}$$

Consider the crystal at low pressure. Similarly, using the method above, the expression for determining the absolute stability limit temperature in the interstitial alloy thin film is developed. At that point,

$$T_s=\frac{r_1}{18\gamma_G k_B}\left[\frac{d\sqrt{3}-3\bar{a}}{d\sqrt{3}+\bar{a}}\sum_X c_X^{tr}\frac{\partial U_{0X}^{tr}}{\partial r_{1X}^{tr}}-\frac{2\bar{a}}{d\sqrt{3}+\bar{a}}\sum_X c_X^{ng}\frac{\partial U_{0X}^{ng}}{\partial r_{1X}^{ng}}-\frac{2\bar{a}}{d\sqrt{3}+\bar{a}}\sum_X c_X^{ng1}\frac{\partial U_{0X}^{ng1}}{\partial r_{1X}^{ng1}}\right]+\left(\frac{\partial T}{\partial P}\right)_{r_1}+... \tag{38}$$

From there, the absolute stability limit temperature T_s (0) in the interstitial alloy thin film state at pressure P = 0 is determined

$$T_s(0)=\frac{r_1}{18\gamma_G k_B}\left[\frac{d\sqrt{3}-3\bar{a}}{d\sqrt{3}+\bar{a}}\sum_X c_X^{tr}\frac{\partial U_{0X}^{tr}}{\partial r_{1X}^{tr}}-\frac{2\bar{a}}{d\sqrt{3}+\bar{a}}\sum_X c_X^{ng}\frac{\partial U_{0X}^{ng}}{\partial r_{1X}^{ng}}-\frac{2\bar{a}}{d\sqrt{3}+\bar{a}}\sum_X c_X^{ng1}\frac{\partial U_{0X}^{ng1}}{\partial r_{1X}^{ng1}}\right], \tag{39}$$

Where the parameters $r_1,\frac{\partial U_{0X}^{m}}{\partial r_{1X}^{m}},\gamma_G,d,\bar{a}(m=tr,ng,ng1)$ are calculated at temperature $T_s(0).$

At pressure P, the absolute stability limit temperature in the interstitial alloy thin film is determined by

$$T_s \approx T_s(0) + \frac{VP}{3k_B(\gamma_G)^2}\left(\frac{\partial \gamma_G}{\partial T}\right)_{r_1} T_s(0). \tag{40}$$

Note that $V, \gamma_G, \frac{\partial \gamma_G}{\partial T}$ are determined at T_s. An approximation of the melting temperature T_m can be considered with T_s. By applying the iterative approximation method to solve the above equation, we obtain better approximate values of T_s at low pressure P.

For a crystal at high pressure, we can calculate the Young's modulus E_Y, the shear modulus G of the interstitial alloy thin film. The isothermal elastic modulus B_T of the interstitial alloy thin film is a function of pressure P, i.e., $B_T = B_T(P)$. At that point, B_T can be expanded into a series

$$B_T(P) = B_{0T} + \left(\frac{dB_{0T}}{dP}\right)_{P=0} P + \frac{1}{2}\left(\frac{d^2 B_{0T}}{dP^2}\right)_{P=0} P^2 + ..., B_{0T} = B_T(P=0). \tag{41}$$

In the first-order approximation $$B_T(P) = B_{0T} + \left(\frac{dB_{0T}}{dP}\right)_{P=0} P. \tag{42}$$

At that point

$$T_m(P) = \frac{T_m(0) B_{0T}^{\frac{1}{B'_{0T}}}}{G(0)} \cdot \frac{G(P)}{(B_{0T} + B'_{0T}P)^{\frac{1}{B'_{0T}}}}, B'_{0T} = \left(\frac{dB_{0T}}{dP}\right)_{P=0}. \tag{43}$$

2.3. Results and discussion

2.3.1. Interaction potential between atoms in the interstitial alloy

To study the interaction between Fe-Fe and Si-Si atoms, we apply the Mie-Lennard-Jones n-m pair potential [19] and the potential parameter values from Table 1.

$$\varphi(r) = \frac{D}{n-m}\left[m\left(\frac{r_0}{r}\right)^n - n\left(\frac{r_0}{r}\right)^m\right], \tag{44}$$

Table 1. The potential parameters D, r_0, m, and n [10] for Fe-Fe, Si-Si interactions.

Interactions	*m*	*n*	$D(10^{-16}\text{erg})$	$r_0(10^{-10}\text{m})$
Fe-Fe	8,26	3,58	12576,70	2,4775
Si-Si	6	12	45128,24	2,295

The interaction potential between Fe-Si atoms is approximated by

$$\varphi_{\text{Fe-Si}} = \frac{1}{2}\left(\varphi_{\text{Fe-Fe}} + \varphi_{\text{Si-Si}}\right). \tag{45}$$

2.3.2. Numerical calculation results for Fe and FeSi thin films

Table 2. The dependence of pressure and number of film layers on the melting temperature for Fe thin films calculated by SMM.

Quantity	*P*(GPa) / n*		**0,5**	**1**	**2**	**3**	**4**	**5**	**6**
			c_{Si} (%) = 0						
$T_m(K)$	SMM	10	1048,64	1055,59	1069,41	1083,07	1096,61	1110,03	1123,32
		20	1442,05	1450,36	1466,86	1483,23	1499,45	1515,53	1531,48
		70	1740,52	1749,87	1768,44	1786,86	1805,14	1823,26	1841,25
		200	1820,67	1830,29	1849,43	1868,41	1887,24	1905,91	1924,45
	[20]	Bulk	1842,5	1873	1908	1943	1978	2013	2033

Table 3. The dependence of silicon concentration and number of film layers on the melting temperature for FeSi thin films at P = 0 calculated by SMM.

Layers	**c_{Si} (%)**	**0**	**1**	**3**	**5**
10	T_m (K)	1041,64	985,60	881,81	788,18
20		1433,70	1355,39	1210,50	1080,00
70		1731,13	1635,92	1459,86	1301,38
200		1811,00	1711,25	1526,82	1360,83

Table 4. The dependence of pressure and silicon concentration on the melting temperature for FeSi thin films at n* = 10 calculated by SMM.

c_{Si} (%)	**P (GPa)**	**0,5**	**1**	**2**	**3**	**4**	**5**	**6**
0	T_m(K)	1048,64	1055,59	1069,41	1083,07	1096,61	1110,03	1123,32
1		994,25	1002,70	1019,17	1035,21	1050,91	1066,32	1081,49
3		893,27	904,29	925,36	945,51	964,98	983,91	1002,39
5		801,88	814,94	839,74	863,26	885,85	907,72	928,98

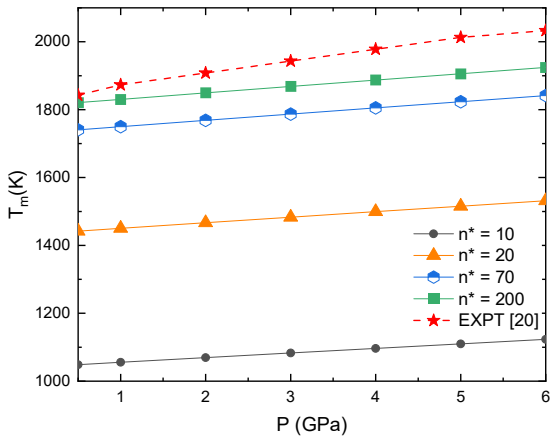

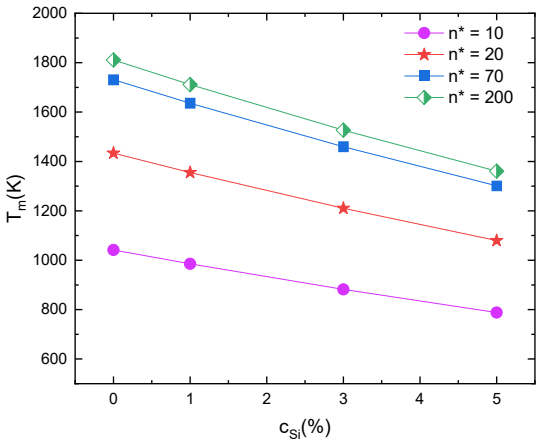

Figure 2. The dependence of pressure and number of film layers on the melting temperature for Fe thin films calculated by SMM.

Figure 3. The dependence of silicon concentration and number of film layers on the melting temperature for FeSi thin films at P = 0 calculated by SMM.

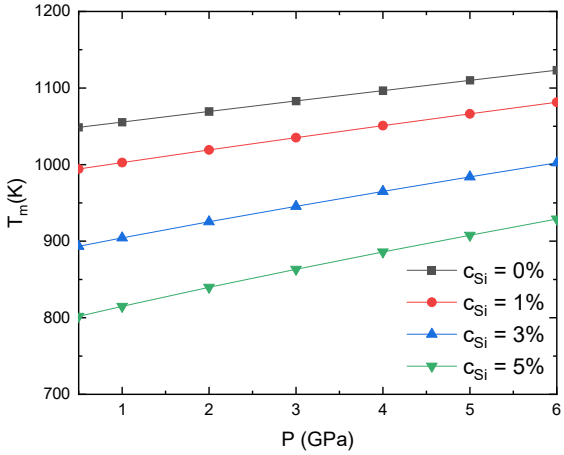

Figure 4. The dependence of pressure and silicon concentration on the melting temperature for FeSi thin films at n* = 10 calculated by SMM.

Figure 2 shows the calculated T_m of the FeSi film. According to the obtained results for a film with 200 layers, corresponding to a film thickness of 70 nm, the T_m of the film gradually approaches the bulk material value [20]. At the same pressure and thickness, T_m increases as the pressure increases. At 10 layers, T_m is 1048,64K increasing sharply to 1740,52K at 70 layers. From 70 layers to 200 layers, T_m increases from 1740,52K to 1820,67K. At P=0.5 GPa, T_m is 1048,64 K for a 10-layer film, increasing to 1820,67 K for a 200-layer film, and approaching the experimental T_m of the bulk material at 1842,5 K. As the film thickness increases, the T_m of the film gradually approaches the T_m of the bulk material [20]. At 200 layers, corresponding to a thickness of 27 nm, T_m = 1820,67K gradually approaches the T_m of the bulk material [20] which is 1842,5K. As the Si concentration increases, Si atoms occupy interstitial sites within the BCC crystal lattice of Fe, causing lattice distortion and disrupting the original crystal order. Due to differences in atomic radius and bonding nature between Fe–Fe and Fe–Si (compared to the original Fe–Fe bonds), the average interatomic bonding strength is weakened, leading to a reduction in bonding energy and consequently lowering the melting temperature. From a thermodynamic perspective, the presence of interstitial atoms increases configurational entropy but simultaneously generates internal stress, rendering the crystal lattice less stable against heating. On the other hand, as pressure increases, the atomic spacing contracts, enhancing the short-range interactions between atoms (particularly modeled by the n–m Mie–Lennard–Jones potential), which in turn raises the bonding energy and stabilizes the lattice. This explains why, at the same Si concentration, the melting temperature increases with pressure.

Figure 3 shows that, for the same number of layers, T_m decreases as the Si concentration increases. For a film with 10 layers and P = 0, T_m is 985,6K at 1% Si concentration, 881,81 K at 3% Si concentration, and 788,18 K at 5% Si concentration. Additionally, at different layers, the T_m values of the film at Si concentrations c_{Si} = 1%, c_{Si} = 3%, and c_{Si} = 5% vary more significantly. For example, in a film with 200 layers, we have T_m = 1711,25 K at c_{Si} = 1%, decreasing to 1526,82 K at c_{Si} = 3%, and further decreasing to 1360,83K at c_{Si} = 5%. This also indicates that, at P = 0 and the same Si concentration, T_m gradually increases with the number of layers. For instance, at c_{Si} = 5%, T_m = 788,18 K at 10 layers, increases to 1301,38 K at 20 layers, and further increases to 1360,83 K at 200 layers. Specifically, from the results in

Tables 2 and 3, we observe that when the number of layers increases from 10 to 70 (corresponding to a thickness increase from approximately 3.5 nm to ~27 nm), the melting temperature (Tm) rises rapidly. However, as the number of layers increases further from 70 to 200 (~70 nm), the increase in Tm slows down and approaches the bulk material value. This indicates that a thickness threshold of around 70 nm marks the transition from the "thin film with distinct properties" region to the "bulk-like material" region. Similarly, Tables 3 and 4 show that with Si concentrations ranging from 0 to 1%, the melting temperature (Tm) decreases slightly; however, once the Si concentration exceeds the threshold of approximately 3%, Tm begins to decrease sharply and continuously. Therefore, 3% can be considered the critical impurity concentration of Si, beyond which the crystal lattice is significantly weakened and undergoes rapid thermal instability. These quantitative thresholds are not easily determined by intuition alone, making the use of the Statistical Moment Method (SMM) to clarify them entirely justified.

Figure 4 shows that the melting temperature of the film decreases as the Si concentration increases. For a 10-layer film at P = 0.5 GPa, T_m decreases from 994,25 K at c_{Si} = 1% to 893,27 K at c_{Si} = 3%, and further down to 801,88 K at c_{Si} = 5%. When the P values are higher, reaching several GPa, the T_m values of the film at different c_{Si} concentrations also show greater differences. For example, at c_{Si} = 5%, T_m = 814,94 K at P = 1 GPa, increases to 863,26 K at P = 3 GPa, and further to 928,98 K at P = 5 GPa. This also indicates that, at the same Si concentration, T_m gradually increases as the pressure increases.

3. Conclusions

This research focuses on developing a model of BCC-structured AB interstitial alloy thin films and advancing the theory of melting temperature using the statistical moment method. Based on the Mie-Lennard-Jones m-n potential and the coordination sphere method, the study determines the melting temperature of Fe and FeSi films within a pressure range of 0.5–6 GPa, interstitial atomic concentrations of 0–5%, and layer counts from 10 to 200. The results indicate that the melting temperature of the films is dependent on pressure, film thickness, and interstitial atomic concentration. As the interstitial atomic concentration approaches 0 or the film thickness becomes sufficiently large, the melting temperature of the film converges towards the bulk material value for the number of layers increases to 200, corresponding to a film thickness of 70 nm. The calculated data are predictive and can provide guidance for experimental studies. This theory can be extended to apply to other metal films, BCC-structured interstitial alloy films, and to advance research on ternary alloys with cubic structures.

References

[1] H. Haibo and F. Spaepen, "Tensilie testing of free – standing Cu, Ag and Al thin films and Ag/Cu multilayers," *Act. Mater.,* vol. 48, no. 12, pp. 3261-3269, Jul. 2000, doi: 10.1016/S1359-6454(00)00128-2.

[2] Sangmoon Park, Benjamin L. Clark, Douglas A. Keszler, Jeffrey P. Bender, John F. Wager, Thomas A. Reynolds, and Gregory S. Herman, "Low-Temperature Thin-Film Deposition and Crystallization," *Mater. Sci.,* vol. 297, no. 5578, p. 65, Jul. 2002, doi: 10.1126/science.1072009.

[3] A. R. Vaz, M. C. Salvadori and M. Cattani, "Young modulus measurement of nanostructured metallic thin films," *Jour. Metas. Nano. Mater.,* Vols. 20-21, pp. 758-762, Jul. 2004, doi: 10.4028/www.scientific.net/JMNM.20-21.758.

[4] B. Weiss, V. Groger, G. Khatibi, A. Kotas, P. Zimprich, R. Stickler and B. Zagar, "Characterization of mechanical and thermal properties of thin Cu foils and wires," *Sen. Act. A,* vol. 99, no. 1-2, pp. 172-182, Apr. 2002, doi: 10.1016/S0924-4247(01)00877-9.

[5] Y. Kuru, M. Wohlschlogel, U. Welzel and E. J. Mittemeijer, "Coefficients of thermal expansion of thin metal films investigated by non-ambient X-ray diffraction stress analysis," *Sur. & Coat. Tech.,* vol. 202, no. 11, pp. 2306-2309, Feb. 2008, doi: 10.1016/j.surfcoat.2007.08.002.

[6] D. Fuks, S. Dorfman, F. Zhukovskii, A. Kotomin and A. M. Stoneham, "Theory of the growth mode for a thin metallic film on an insulating substrate," *Sur. Sci.,* vol. 499, no. 1, pp. 24-40, Feb. 2002, doi: 10.1016/S0039-

6028(01)01692-2.
[7] Richard P. Vinci & Joost J. Vlassak, "Mechanical behavior of thin films," *Annu. Rev. Mater. Sci.,* vol. 26, pp. 431-462, Aug. 1996, doi: 10.1146/annurev.ms.26.080196.002243.
[8] Vu Van Hung, Duong Dai Phuong and Nguyen Thi Hoa, "Investigation of thermodynamic properties of metal thin film by statistical moment method," *Com. Phys.,* vol. 23, no. 4, pp. 301–311, Feb. 2014, doi: 10.15625/0868-3166/23/4/3351.
[9] Vu Van Hung, Duong Dai Phuong and Nguyen Thi Hoa, "Thermodynamic properties of free standing thin metal films: Temperature and pressure dependences," *Com. Phys.,* vol. 24, no. 2, pp. 177–191, Jul. 2014, doi: 10.15625/0868-3166/24/2/177/3731.
[10] M. N. Magomedov , "The calculation of the parameters of the mie-lennard jones potential," *High Temp.,* vol. 44, no. 4, pp. 513-529, Jul. 2006, doi: 10.1007/s10740-006-0064-5.
[11] S. M. Rezende, J. A. S. Moura, W. H. Schreiner and F. M. de Aguiar, "Ferromagnetic resonance of Fe(111) thin films and Fe(111)/Cu(111) multilayers," *Phys. Rev. B,* vol. 49, no. 21, Jun. 1994, doi: 10.1103/PhysRevB.49.15105.
[12] A.F. Guillermet & P. Gustafson, "An assessment of the thermodynamic properties and the (p, T) phase diagram of iron," *High Temp-High Press,* vol. 16, no. 6, pp. 591-610, 1984.
[13] Nguyen Quang Hoc, Bui Duc Tinh and Nguyen Duc Hien, "Elastic moduli and elastic constants of interstitial alloy AuCuSi with FCC structure under pressure," *High Temp. Mater. Proc.,* vol. 38, pp. 264–272, Sep. 2018, doi: 10.1515/htmp-2018-0027.
[14] Duong Dai Phuong, Nguyen Thi Hoa, Vu Van Hung, Doan Quoc Khoa, Ho Khac Hieu, "Mechanical properties of metallic thin films: Theoretical approach," *The Eur. Phys. Jour. B,* vol. 89, no. 3, pp. 1–7, Mar. 2016, doi: 10.1140/epjb/e2016-60583-y.
[15] Vu Van Hung, Statistical method of moment in studying thermodynamic and elastic properties of crystals, Hanoi: University of Education Publishing House, 2009.
[16] Bui Duc Tinh, Nguyen Quang Hoc, Dinh Quang Vinh, Tran Duc Cuong and Nguyen Duc Hien, "Thermodynamic and elastic properties of interstitial alloy FeC with BCC structure at zero pressure," *Adv. Mater. Sci. Eng.,* vol. 2018, no. 4, pp. 1–8, Oct. 2018, doi: 10.1155/2018/5251741.
[17] Nguyen Tang and Vu Van Hung, "Investigation of the thermodynamic properties of anharmonic crystals by the momentum method, I. General results for FCC crystals," *Phys. Stat. Sol. (b),* vol. 149, no. 2, pp. 511–519, Oct. 1988, doi: 10.1002/pssb.2221490212.
[18] R. Knepper and S. P. Baker, "Coefficient of thermal expansion and biaxial elastic modulus of β phase tantalum thin films," *Appl. Phys. Lett.,* vol. 90, no. 18, Apr. 2007, doi: 10.1063/1.2734468.
[19] M. N. Magomedov, "On calculating the Debye temperature and the Gruneisen parameter," *Russ. J. Phys. Chem. A,* vol. 61, p. 1003–1009., 1987. (In Russian).
[20] E. Y. Tonkov and E. G. Ponyatovsky, Phase transformations of elements under high pressure, USA: CRC Press, Jan. 2004, doi: 10.1201/9781420037609.